

Lateral plasmonic superlattice in strongly dissipative regime

I. V. Gorbenko¹ and V. Yu. Kachorovskii¹

¹*Ioffe Institute, 194021 St. Petersburg, Russia*

We calculate transmission coefficient, \mathcal{T} , of terahertz radiation through lateral plasmonic superlattice with a unit cell consisting of two regions with different plasma wave velocities, s_1 and s_2 ($s_1 > s_2$). We generalize theory developed earlier for resonant case to the non-resonant regime, when the scattering rate, γ , is large compared to fundamental gate-tunable frequencies $\omega_{1,2}$ of plasma oscillations in both regions. We find that absorption, and consequently \mathcal{T} , strongly depends on density modulation amplitude and on the frequency of the incoming radiation. We describe evolution of the absorption with increasing of radiation frequency from the quasi-static regime of very low frequency to the high-frequency regime, identify several dissipation regimes and find analytical expression for absorption, and, accordingly, for \mathcal{T} , in these regimes. A general phase diagram of non-resonant regime in the plane (ω, ω_2) for fixed ω_1 is constructed. Most importantly, \mathcal{T} sharply depends on the gate voltages and frequency. In particular, for $\omega_2 \ll \omega_1$, \mathcal{T} strongly varies on the very small frequency scale, $\delta\omega \ll \gamma$, determined by the Maxwell relaxation, $\delta\omega \sim \omega_1^2/\gamma$, so that the superlattice shows high responsivity within the frequency band $\delta\omega$.

I. INTRODUCTION

Exploration of plasma waves in two-dimensional (2D) systems, which began in 1970s [1–8], was initiated by theoretical analysis of spectrum of 2D plasma waves [1] and first experimental observation of 2D plasmons in infrared light absorption in 2D electron gas with grating couplers [2].

Plasmonic oscillations are not only of fundamental interest, but are also very promising for applications (for review, see [9]). Remarkably, in 2D gated structures, the plasma wave velocity s can be tuned by the gate voltage and its typical value, $s \sim 10^8$ cm/s, exceeds by the order of magnitude the electron drift velocity $\lesssim 10^7$ cm/s. Hence, for semiconductor structures with submicron sizes, the frequency of plasmon oscillations falls in the terahertz (THz) range. This opens a wide avenue to create tunable semiconductor devices operating in the THz range of frequencies.

A significant boost supporting the idea of 2D THz plasmonics was given by Dyakonov and Shur, who proposed dc-current-driven plasma waves instability mechanism in the field-effect transistor (FET) [10] and have also shown that FET can be used as tunable detector, resonant or non-resonant, of the THz radiation [11]. These works initiated a series of publications focused on the theoretical, experimental and numerical study of plasma wave phenomena in FETs (see reviews [12–14] and references therein).

Quite soon it became clear that multi-gated 2D structures, where electron density is modulated with period L (typical value $\sim 1 \mu\text{m}$), have significant advantages as compared to single FETs. In particular, for a given value of L , coupling of system with THz radiation (with a typical wavelength $100 \mu\text{m}$) increases with number of gratings, i.e. number of modulation periods. Experimentally, in these structures transmission coefficient shows plasmonic resonances of good quality up to 170 K in AlGaIn/GaN-based structures [15] and up to the room temperature in grating-gate graphene structures [16].

The grating-gate FETs are of particular interest also from the fundamental point of view. The periodical density modulation creates crystal structure for plasma waves with pass and stop bands tunable by the gate voltage. Hence, such structure represents lateral plasmonic crystal (LPC) with the unique possibility of pure electrical control of the band structure. Such LPC are actively studied theoretically and numerically [17–23], as well as experimentally [15, 16, 24–26]. Very recently, the possibility of tuning LPC from weak to strong coupling regime by gate voltage was verified experimentally [26] and described theoretically [27], with a good agreement between experiment and theory.

The study of non-resonant regime of LPC operation, when widths of pass- and stop-bands of LPC are smaller than the momentum relaxation rate, is also of very significant interest. It is worth noting that the most intense response in single FETs is usually experimentally obtained in the non-resonant regime, when FET channel is depleted, as was first demonstrated in Ref. [28] (for review of more recent publications discussing non-resonant regime, see Ref. [29–34]). Moreover, in the non-resonant regime, a giant dc-current-induced increase of direct voltage response [35] and polarization-sensitive plasma wave interference effects [36–39] were demonstrated both theoretically and experimentally. Also, the appearance of dc current in modulated systems without center of inversion—the so called ratchet effect—is actively studied in LPC systems, in particular, in the non-resonant regime [20, 40–47]. As for the transmission coefficient through such a crystal, even for good structures, where it shows good plasmon resonances for lowest plasmonic modes, the high-order resonances are significantly suppressed by dissipation [15, 16, 26], so that they should be described by non-resonant theory.

In this paper we calculate transmission coefficient connected with absorption of the THz radiation in lateral plasmonic crystal operating in the non-resonant regime. We identify several dissipation regimes and find analytical expression for absorption, and, consequently, for

transmission coefficient in these regimes.

II. MODEL

A. Problem formulation and general approach

We follow recent works [16–18, 27] and describe lateral plasmonic crystal as a system of alternating stripes with a unit cell consisting from two regions with lengths L_1 and L_2 ($L_1 + L_2 = L$) having plasma wave velocities s_1 and s_2 ($s_1 > s_2$), and operating in the non-resonant regime: $\gamma \gg \omega_1$, $\gamma \gg \omega_2$, where γ is the momentum relaxation rate and $\omega_{1,2} = \pi s_{1,2}/L_{1,2}$. For such conditions, plasma resonance are damped. The purpose of this work is to construct a general phase diagram of non-resonant regime in the plane (ω, ω_2) (for fixed ω_1) depending on gate-tunable frequencies $(s_1/L_1, s_2/L_2)$. To be specific, we fix s_1 and assume that s_2 can be tuned by gate in the interval $0 < s_2 < s_1$ (hence ω_2 changes from 0 to ω_1 if we put $L_1 = L_2$). Following Ref. [16], we refer to region “1” as *active* and to region “2” – as *passive*. The case $|s_1 - s_2| \ll s_1$ corresponds to the weak coupling of the LPC, when electron density is weakly modulated. The opposite case of the strong coupling, i.e. strong density modulation, is realized for $s_2 \ll s_1$.

We assume that system is illuminated with THz radiation, which can be assumed homogeneous due to large wavelength, and calculate transmission spectrum up to the first order of σ/c with c – the speed of light and σ – 2D electron liquid conductivity.

In this case, one can neglect radiative decay of plasmonic oscillations (see Refs. [16, 48]) and transmission coefficient is close to unity with a small correction, which is fully expressed in terms of Ohmic dissipation in the channel, P :

$$\mathcal{T} \approx 1 - \frac{8\pi P}{c\sqrt{\epsilon}E_0^2}, \quad (1)$$

where E_0 is the amplitude of the incoming radiation, and ϵ is the dielectric constant.

Local dissipation within hydrodynamic approximation is given by $m|\mathbf{v}(x, t)|^2/\tau$ [41], where $\mathbf{v}(x, t)$ is the hydrodynamic velocity and τ is the momentum relaxation time. Hence, the ohmic dissipation per unit area in a plasmonic crystal reads

$$P = \left\langle N \frac{m|\mathbf{v}(x, t)|^2}{\tau} \right\rangle_{x,t} \quad (2)$$

where $N = N(x, t)$ is the electron concentration in the channel and $\langle \dots \rangle_{x,t}$ stands for averaging taken over area of the crystal and period of the incoming radiation.

Now let us discuss external field properties. Grating gate modulates not only electron concentration but also amplitude of electromagnetic field. So the field in the channel is a sum of homogeneous plane wave and

evanescent waves modulated with a period of grating $L = L_1 + L_2$.

Effect of grating field modulation, was discussed in details for resonant and so-called super-resonant regimes [27] within the simplified model proposed in Ref.[40]. Most importantly, due to the inhomogeneous component, a number of *dark* plasmonic modes, which are not coupled to homogeneous field, can be excited.

The dark modes have not yet been observed experimentally neither in FETs, nor in LPC. Moreover we have recently shown theoretically [27] that such modes can be only excited provided that field modulation violates inversion symmetry of the whole system (this effect can be taken into account by introducing a phase shift between modulations of the external field and concentration). For the case when phase shift is zero, dark modes are not excited and field modulation only leads to small corrections to amplitudes of bright modes. Therefore, as first approximation, one can neglect these corrections and consider homogeneous excitation $E(t) = E_0 \cos(\omega t)$.

B. Hydrodynamic approximation

In this paper, we describe LPC by using hydrodynamic approximation, so that we assume that the electron-electron collisions dominate over impurity and phonon scattering and 2D electron liquid in the channel can be described by Euler and continuity equations.

$$\frac{\partial v}{\partial t} + v \frac{\partial v}{\partial x} + \gamma v = -\frac{e}{m} \frac{\partial U}{\partial x} + \frac{F}{m}, \quad (3)$$

$$\frac{\partial U}{\partial t} + \frac{\partial}{\partial x}(Uv) = 0, \quad (4)$$

with local drift velocity $v(x, t)$, and local gate-to-channel voltage $U(x, t)$. Equilibrium electron concentration in the channel is controlled with gate voltage U_g :

$$N_0 = \frac{C(U_g - U_{th})}{e}, \quad (5)$$

while the local concentration is given by the same equation with replacement $U_g \rightarrow U(x, t)$. Here U_{th} is the threshold voltage, $C = \epsilon/4\pi d$ is the channel capacitance per unit area, and d is the spacer width. Plasmonic effects are connected with the term $(e/m)\partial U/\partial x$ in Eq. (3). The plasma wave velocity depends on the concentration and, consequently, is also gate-tunable:

$$s = \sqrt{\frac{e(U_g - U_{th})}{m}}. \quad (6)$$

Standard boundary conditions between active and passive regions [17, 18] correspond to conservation of the current, Nv , and energy flux, $mv^2/2 + eU$. We neglect in hydrodynamic equations viscosity, η , assuming that $\eta q^2 \ll \gamma$ (here $q \sim 1/L$), so that impurity scattering dominates over viscous friction. The calculation are rather

standard, so we present here the results, while the specific details can be found in Ref.[27]. Direct calculation of dissipation yields

$$P = \frac{\gamma^2}{\omega^2 + \gamma^2} [P_0 + P_{\text{res}}], \quad (7)$$

where

$$P_0 = \frac{F_0^2 C}{2e^2 \gamma (L_1 + L_2)} (L_1 s_1^2 + L_2 s_2^2), \quad (8)$$

$$P_{\text{res}} = \frac{F_0^2 C}{2e^2 (L_1 + L_2)} \frac{(s_1^2 - s_2^2)^2 \text{Re} [(\Gamma - i\Omega)^3 \Sigma]}{\Omega \Gamma (\Gamma^2 + \Omega^2) |\Sigma|^2}. \quad (9)$$

Here

$$\Sigma = s_1 \cot q_1 L_1 / 2 + s_2 \cot q_2 L_2 / 2, \quad (10)$$

depends on complex wave vectors,

$$q_{1,2} = \frac{\sqrt{\omega(\omega + i\gamma)}}{s_{1,2}} = \frac{\Omega + i\Gamma}{s_{1,2}}, \quad (11)$$

where Ω and Γ describe, respectively, frequency and damping of density oscillations. The complex wave vectors are different in regions “1” and “2” ($q_1 \neq q_2$) due to different plasma velocities $s_{1,2}$, while Ω and Γ are the same in both regions if γ is constant across the PC.

In the resonant regime, when γ is small, the dissipation P shows sharp maxima, the positions of which can be found by sending $\gamma \rightarrow 0$. Then Σ becomes real and has exact zeros at frequencies that determine plasmonic resonances.

We also note that

$$\begin{aligned} P(s_2 = s_1) &= \frac{\gamma^2}{\omega^2 + \gamma^2} P_0(s_2 = s_1) \\ &= P_{\text{Dr}} = \frac{\gamma F_0^2 C s_1^2}{2e^2 (\omega^2 + \gamma^2)}. \end{aligned} \quad (12)$$

C. Damping of plasma waves

Wave vectors $q_{1,2}$ depend on plasma wave velocities $s_{1,2}$ and have real and imaginary parts determined by $\Omega = \Omega(\omega, \gamma)$ and $\Gamma = \Gamma(\omega, \gamma)$, respectively. The imaginary parts determine spatial rate of plasma oscillations damping so we introduce the characteristic lengths $L_{1,2}^* = s_{1,2}/\Gamma$. From Eq. (11), we find

$$\Omega = \left[\frac{\gamma^2/2}{\sqrt{1 + \gamma^2/\omega^2} - 1} \right]^{1/2} \approx \begin{cases} \omega & \text{for } \omega \gg \gamma, \\ \sqrt{\omega\gamma/2} & \text{for } \omega \ll \gamma, \end{cases} \quad (13)$$

$$\Gamma = \left[\frac{\gamma^2/2}{\sqrt{1 + \gamma^2/\omega^2} + 1} \right]^{1/2} \approx \begin{cases} \gamma/2 & \text{for } \omega \gg \gamma, \\ \sqrt{\omega\gamma/2} & \text{for } \omega \ll \gamma. \end{cases} \quad (14)$$

Hence, $q_{1,2} \approx (1 + i) \sqrt{\omega\gamma/2}/s_{1,2}$ for low frequency, $\omega \ll \gamma$, and $q_{1,2} \approx (\omega + i\gamma/2)/s_{1,2}$, for high frequency, $\omega \gg \gamma$. Therefore, the dissipation lengths read

$$L_{1,2}^* \approx \begin{cases} 2s_{1,2}/\gamma & \text{for } \omega \gg \gamma, \\ \sqrt{2}s_{1,2}/\sqrt{\omega\gamma} & \text{for } \omega \ll \gamma. \end{cases} \quad (15)$$

Both 1 and 2 regions can be “long” or “short” depending on the relation between L_i and L_i^* , $i = (1, 2)$. For *long region* ($L_i^* \ll L_i$, i.e. $\omega \gg \omega_i^2/\gamma$) plasma waves rapidly decay from boundaries inside the region i . For *short region* ($L_i^* \gg L_i$, i.e. $\omega \ll \omega_i^2/\gamma$) the plasma wave also decays exponentially, but the length of decay is much larger than length of strip, so amplitude of plasma wave doesn’t change much. This regime also includes quasi-static regime of operation, when the external frequency is very low $\omega \ll \omega_2^2/\gamma < \omega_1^2/\gamma \ll \gamma$, so that both 1 and 2 regions turn out to be short.

Importantly, for $s_1 \gg s_2$ and $L_1 \sim L_2$ there is an *intermediate* regime, when $L_1^* \gg L_1$ and at the same time $L_2^* \ll L_2$ ($\omega_2^2/\gamma \ll \omega \ll \omega_1^2/\gamma$). For such case, plasmonic oscillations in regions 1 have approximately constant amplitude but rapidly decay into regions 2, so that plasmonic oscillations in different regions 1 are effectively disconnected (hence, terms “active” and “passive” with respect to stripes 1 and 2). In this regime, there are two competing contributions to the dissipation, from plasmonic oscillations in regions 1 and also from narrow boundary regions $\sim L_2^*$ in the stripes 2. As we will see, in some excitation regimes the second contribution can dominate.

III. FREQUENCY DEPENDENCE OF DISSIPATION

Next, we discuss evolution of the dissipation with increasing of excitation frequency.

As follows from Eq. (15), lengths $L_{1,2}^*$ decay with frequency. At very low frequency, both 1 and 2 regions are short, $L_1^* \gg L_1$, $L_2^* \gg L_2$. We will call this regime as “short cell” regime. In this quasi-static regime, the system dissipates according to the static Ohm’s law. In the opposite limit of very high frequency $L_1^* \ll L_1$, $L_2^* \ll L_2$, plasma oscillations are overdamped and are spatially limited to very narrow layers on the inter-regions boundaries. In this case, which we will call “long sell” regime, the main contribution to the dissipation is related to homogeneous Drude dissipation in the external field. Below, we discuss in more detail these regimes as well as a number of other intermediate regimes.

Linearization of Eqs. (3) and (4) leads to the following equation, that gives position of plasmonic resonances in the response to an external force of frequency ω :

$$[\omega^2 - \omega_q^2]^2 \tau^2 + \omega^2 = 0. \quad (16)$$

Here $\omega_q = qs$ and $\tau = \gamma^{-1}$. For a stripe of width L , wave vector q is quantized and the fundamental frequency is

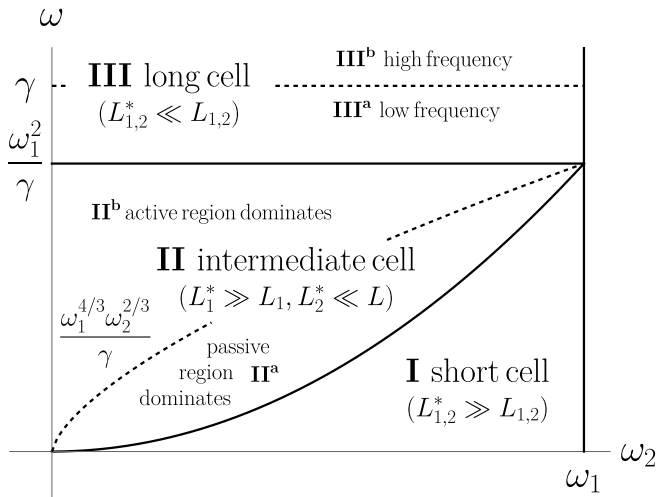


FIG. 1. Different regimes of dissipation in nonresonant PC ($\gamma \gg \omega_{1,2}$) schematically presented on a (ω, ω_2) -plane while γ and ω_1 are fixed and $\gamma \gg \omega_1 \geq \omega_2$. Here we assume $L_1 \sim L_2$ and omit numerical coefficients. Thick lines divide diagram into three regimes: (I) short cell, (II) intermediate cell and (III) long cell. Condition $L_2^* = L_2$ defines boundary between (I) and (II) ($\omega = \omega_2^2/\gamma$). Analogically, line between (II) and (III) is found from $L_1^* = L_1$ ($\omega = \omega_1^2/\gamma$). Dashed line $\omega = \gamma$ splits regime (III) into high and low frequency regimes. Dashed line $\omega^3 = \omega_1^4 \omega_2^3 / \gamma^3$ separates region II into sub-regions of (II^b) and (II^a), where dominant contribution to the dissipation is given by plasmonic oscillations in the active region or exponentially decaying tails in the passive regions, respectively.

determined by $q = \pi/L$. For large τ , this equation gives $\omega \approx \omega_q - i\gamma/2$. However, in the non-resonant regime, when $\omega\tau \ll 1$ and $\omega_q\tau \ll 1$, this equation determines the Maxwell relaxation rate instead of frequency of plasmonic resonances:

$$\omega = \pm i\omega_q^2\tau. \quad (17)$$

Hence, two relaxation rates appear in the problem

$$\Gamma_{1,2} = \omega_{q_{1,2}}^2/\gamma \ll \gamma. \quad (18)$$

These rates have a physical meaning of the Maxwell relaxation rates in the passive and active regions.

A. “Short cell” regime (see region I at Fig.1 and Fig.2)

In the quasi-static regime, we have

$$\Omega \approx \Gamma \approx \sqrt{\omega\gamma/2}, \quad \Sigma \approx \frac{\sqrt{2}(1-i)}{\sqrt{\omega\gamma}} \left(\frac{s_1^2}{L_1} + \frac{s_2^2}{L_2} \right), \quad (19)$$

and $L_1^* \gg L_1, L_2^* \gg L_2$. Using these formulas, one can expand Eq. (9) over ω up to the second order. The results

reads (for simplicity here we take $L_1 = L_2 = L/2$):

$$P = P_0 \left[\frac{2s_1s_2}{s_1^2 + s_2^2} \right]^2 \left[1 + \omega^2\xi \frac{\gamma^2(1-k^2)^2}{\omega_2^4} - \frac{\omega^2}{\gamma^2} \right]. \quad (20)$$

Here $k = s_2/s_1$ ($0 \leq k \leq 1$) and $\xi = \pi^4(k^4 + 22k^2 + 1)/2880(1+k^2)^2$ ($0.03 < \xi < 0.21$). The first term in the square brackets corresponds to the quasi-static Ohm’s law, while term $\propto \gamma^{-2}$ comes from the expansion of the Drude factor: $\gamma^2/(\gamma^2 + \omega^2) \approx 1 - \omega^2/\gamma^2$. It worth noting that dissipation at zero frequency strongly depends on type of LPC coupling: for weak coupling ($s_1 \approx s_2$) $P(0) \approx P_0$, while for strong coupling ($s_1 \gg s_2$), dissipation is much lower due to blocking of dc current in the zero-frequency limit by low-conducting passive regions: $P(0) \approx P_0 s_2^2/s_1^2$.

The term $\propto \xi$ describes retardation related to the Maxwell relaxation in the passive stripe. We see that there are two corrections, which are proportional to ω^2 and have different signs. For $s_1 \sim s_2$ ($k \sim 1$) the term $\propto \xi$ is larger and the ω^2 -correction is positive. However, in the weak coupling regime, when k turns to unity, the ω^2 -correction can change sign. Assuming now arbitrary L_1 and L_2 and denoting $\delta s = s_1 - s_2$, for weak coupling regime $\delta s \ll s_1$, the relative correction is

$$\frac{P(\omega) - P(0)}{P(0)} = -\frac{\omega^2}{\gamma^2} + \frac{\delta s^2 \gamma^2 L_1^* L_2^* (L_1^2 + 4L_1 L_2 + L_2^2)}{180(L_1 + L_2)^2 s_1^6} \omega^2.$$

For $L_1 = L_2 = L/2$ change of sign happens for plasma wave velocity modulation $\delta s/s_1 = 2\sqrt{30}\omega_1^2/\gamma^2\pi^3 \approx 1.1 \omega_1^2/\gamma^2$.

B. “Intermediate cell” regime (see region II at Fig.1 and Fig.2)

In this regime

$$\Omega \approx \Gamma \approx \sqrt{\omega\gamma/2}, \quad \Sigma \approx -is_2 + \frac{(1-i)s_1^2}{\sqrt{\omega\gamma}L_1}, \quad (21)$$

$L_2^* \ll L_2, L_1^* \gg L_1$, and plasma waves existing in the active regions exponentially decay into region “2” from the inter-region boundaries. Conditions on frequency of intermediate cell regime read $\omega_2 \ll \sqrt{\omega\gamma} \ll \omega_1$. Keeping in mind that $\omega \ll \gamma$ we find from Eq. (9)

$$P = P_0 \frac{\pi^4}{120} \frac{\omega^2 \gamma^2 L_1}{\omega_1^4 (L_1 + L_2)} + P_0 \left[\frac{(2L_1 + L_2)s_2^2}{L_1 s_1^2 + L_2 s_2^2} + \frac{\sqrt{\omega\gamma} L_1^2 s_2}{2\sqrt{2}(L_1 s_1^2 + L_2 s_2^2)} \right] \quad (22)$$

First term, proportional to ω^2 , represents contribution to the dissipation from the active region, where $L_1^* \gg L_1$. Physically, this term is responsible for retardation effect related to the Maxwell relaxation in the active regions. The frequency-dependent term, $\propto \sqrt{\omega}$, in the

square brackets describes dissipation within boundary regions on the order L_2^* in the passive regions. These two terms compete with each other, so that either passive or active region can dominate in the dissipation. Equalizing the terms proportional to ω^2 and $\sqrt{\omega}$, and assuming $L_1 = L_2 = L/2$ one gets

$$\omega = \omega^* = \left(\frac{1800 \omega_1^4 \omega_2^2}{\pi^6 \gamma^3} \right)^{1/3} \approx 1.24 \frac{\omega_1^{4/3} \omega_2^{2/3}}{\gamma}.$$

For $\omega \gg \omega^*$ the term, proportional to ω^2 , is larger, so that dissipation in active region gives the leading contribution (see region II^b at Fig.1 and Fig.2). The contribution of passive regions can be neglected and the system without loss of generality can be considered as an array of active strips separated by insulating regions.

For smaller frequency $\omega \ll \omega^*$, the term which is $\propto \sqrt{\omega}$ dominates. This contribution comes from exponentially decaying plasma waves in region "2".

C. "Long cell" regime, (see region III at Fig.1 and Fig.2)

In this case, plasma waves exponentially decay in both active and passive regions: $L_{1,2}^* \ll L_{1,2}$, i.e. $\omega \gg \omega_{1,2}^2/\gamma$. Physically this means, that in both regions the time of the Maxwell relaxation becomes larger than the period of the external field oscillation. The dissipation in this case is given by the following equation

$$P = \frac{P_0 \gamma^2}{\omega^2 + \gamma^2} \left[1 - \frac{(s_1 - s_2)^2 (s_1 + s_2) (3\Gamma^2 - \Omega^2)}{\Gamma(\Gamma^2 + \Omega^2)(L_1 s_1^2 + L_2 s_2^2)} \right], \quad (23)$$

which is the product of the Drude dissipation in the homogeneous external field and a factor in square brackets, which slowly increase with ω due to correction caused by finite length of the boundary layer. The latter is negative at relatively low frequency and saturates at positive value for very high frequencies, where ω becomes larger than γ , so that plasmon damping length saturates on the value s_1/γ for $\omega \rightarrow \infty$. Hence, there are two regions III^a and III^b at Figs.1 and 2.

1. Low frequency, region III^a at Fig.1 and Fig.2

For $\omega_1^2/\gamma \ll \omega \ll \gamma$, we get

$$\Omega \approx \Gamma \approx \sqrt{\omega\gamma/2}, \quad \Sigma \approx -i(s_2 + s_2) \quad (24)$$

and Eq.23 simplifies:

$$P \approx P_0 \left[1 - \frac{\sqrt{2}(s_1 - s_2)^2 (s_1 + s_2)}{\sqrt{\omega\gamma}(L_1 s_1^2 + L_2 s_2^2)} - \frac{\omega^2}{\gamma^2} \right]. \quad (25)$$

Two frequency-dependent terms in the square brackets represent small corrections, which yield the maximum of

P (see Fig. 2). For $s_2 \ll s_1$, dissipation is maximal at $\omega \sim \omega_1^{2/5} \gamma^{3/5}$.

Introducing $L_{\text{eff}} = (L_1 s_1^2 + L_2 s_2^2)/s_1^2$ ($L_{\text{eff}}|_{s_2=s_1} = L_1 + L_2$, $L_{\text{eff}}|_{s_2=0} = L_1$), one can rewrite Eq. (25) as follows

$$P = P_0 \left[1 - \left(1 - \frac{s_2}{s_1} \right)^2 \frac{L_1^* + L_2^*}{L_{\text{eff}}} - \frac{\omega^2}{\gamma^2} \right]. \quad (26)$$

We also note that in the isolated strip ($s_2 = 0$) $P = P_0(1 - L_1^*/L_1 - \omega^2/\gamma^2)$ and in the homogeneous system ($s_2 = s_1$), dissipation is given by the Drude formula.

2. High frequency, region III^b at Fig.1 and Fig.2

When external frequency exceeds γ , damping of plasma waves saturates

$$\Omega \approx \omega, \quad \Gamma \approx \gamma/2, \quad \Sigma \approx -i(s_2 + s_2). \quad (27)$$

and Eq. (23) becomes

$$P = \frac{\gamma^2}{\omega^2} P_0 \left[1 + \frac{2(s_1 - s_2)^2 (s_1 + s_2)}{\gamma(L_1 s_1^2 + L_2 s_2^2)} \right]. \quad (28)$$

It is worth noting that the second term in the square brackets is small frequency-independent correction which have opposite sign to $1/\sqrt{\omega}$ - correction in Eq. (25). This correction comes from the narrow region of width s/γ near the boundary.

IV. DISCUSSION AND CONCLUSION

Analyzing results obtained above we conclude that the most interesting effects are related to the Maxwell relaxation. Remarkably, in the strongly dissipative regime under discussion, the rates of the Maxwell relaxation are much smaller than the dissipation rate: $\Gamma_{1,2} \ll \gamma$. On the other hand, these rates describe characteristic scales of variation P with frequency. In particular, in the region II^b, dissipation sharply increase with ω within the frequency interval on the order of $\Gamma_1 \ll \gamma$. Consequently, $P(\omega)$ has a sharp minimum with a width $\sim \Gamma_1$, and this resonance is better seen if we re-plot Fig. 2 in normal (not log-log) scale.

To conclude, we have studied the transmission of the THz radiation through the lateral plasmonic superlattice with a unit cell consisting from two regions with different plasma wave velocities. We have developed a theory of the non-resonant absorption and described evolution with increasing radiation frequency. Several absorption regimes are identified, described analytically and illustrated on the general diagram. It is demonstrated that although being deeply in the non-resonant regime, the system in strong coupling shows very sharp dependence on the frequency within the very small frequency scale, ω_1^2/γ determined by the Maxwell relaxation, which is

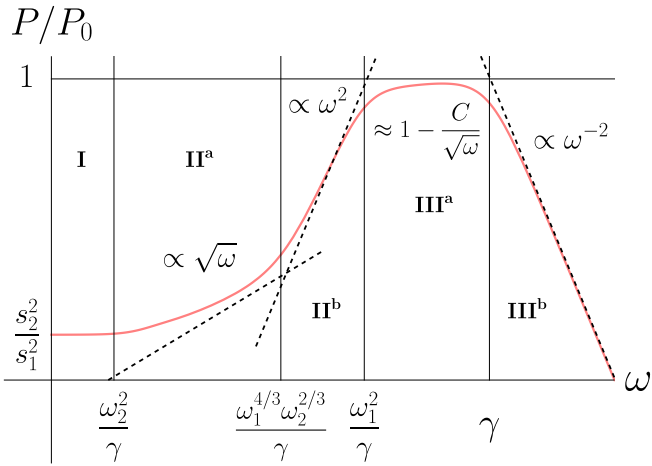


FIG. 2. Different regimes of dissipation in nonresonant PC ($\gamma \gg \omega_{1,2}$) at log-log plot of normalized dissipation on frequency (red line). Frequencies labeled at horizontal axis together with vertical dashed lines represent boundaries of described regimes. Value $P/P_0 = s_2^2/s_1^2$ represents approximation of zero-frequency dissipation in strong coupling regime. With dashed lines at regions II^a, II^b and III^b we draw asymptotics $\sqrt{\omega}$, ω^2 and ω^{-2} correspondingly. We omit numerical values when label both axis; dissipation is plotted using $L_1 = L_2$, $\omega_2/\omega_1 = 0.01$, $\omega_1/\gamma = 0.1$; $C \approx 2\sqrt{2}s_1/L\sqrt{\gamma}$

much smaller than the damping rate γ . The responsivity of the system with respect to gate voltages strongly increases in this frequency domain.

ACKNOWLEDGEMENTS

We thank S. L. Rumyantsev for very useful discussions. The work was supported by the Russian Science Foundation under grant 24-62-00010. The work of I.G. was also partially supported by the Theoretical Physics and Mathematics Advancement Foundation “BASIS”.

-
- [1] A. V. Chaplik, Sov. Phys. JETP **35**, 395 (1972).
 - [2] S. J. Allen, D. C. Tsui, and R. A. Logan, Phys. Rev. Lett. **38**, 980 (1977).
 - [3] T. Theis, J. Kotthaus, and P. Stiles, Solid State Commun. **24**, 273 (1977).
 - [4] D. Tsui, S. Allen, R. Logan, A. Kamgar, and S. Copper-smith, Surf. Sci. **73**, 419 (1978).
 - [5] T. Theis, J. Kotthaus, and P. Stiles, Solid State Commun. **26**, 603 (1978).
 - [6] T. N. Theis, Surf. Sci. **98**, 515 (1980).
 - [7] D. Tsui, E. Gornik, and R. Logan, Solid State Commun. **35**, 875 (1980).
 - [8] J. Kotthaus, W. Hansen, H. Pohlmann, M. Wassermeier, and K. Ploog, Surface Science **196**, 600 (1988).
 - [9] S. Maier, *Plasmonics - Fundamentals and Applications* (Springer, 2007).
 - [10] M. Dyakonov and M. Shur, Phys. Rev. Lett. **71**, 2465 (1993).
 - [11] M. Dyakonov and M. Shur, IEEE Transactions on Electron Devices **43**, 380 (1996).
 - [12] T. Otsuji and M. Shur, IEEE Microwave Magazine **15**, 43–50 (2014).
 - [13] N. Akter, N. Pala, W. Knap, and M. Shur, “Thz plasma field effect transistor detectors,” (2021).
 - [14] M. Shur, G. Aizin, T. Otsuji, and V. Ryzhii, Sensors **21**, 7907 (2021).
 - [15] A. V. Muravjov, D. B. Veksler, V. V. Popov, O. V. Polischuk, N. Pala, X. Hu, R. Gaska, H. Saxena, R. E. Peale, and M. S. Shur, Applied Physics Letters **96**, 042105 (2010).
 - [16] S. Boubanga-Tombet, W. Knap, D. Yadav, A. Satou, D. B. But, V. V. Popov, I. V. Gorbenko, V. Kachorovskii, and T. Otsuji, Phys. Rev. X **10**, 031004 (2020).
 - [17] V. Y. Kachorovskii and M. S. Shur, Applied Physics Letters **100**, 232108 (2012).
 - [18] A. S. Petrov, D. Svintsov, V. Ryzhii, and M. S. Shur, Phys. Rev. B **95**, 045405 (2017).
 - [19] G. R. Aizin, J. Mikalopas, and M. Shur, Phys. Rev. B **107**, 245424 (2023).
 - [20] V. V. Popov, D. V. Fateev, T. Otsuji, Y. M. Meziani, D. Coquillat, and W. Knap, Applied Physics Letters **99**, 243504 (2011).
 - [21] V. V. Popov, D. V. Fateev, E. L. Ivchenko, and S. D. Ganichev, Physical Review B **91**, 235436 (2015).
 - [22] D. V. Fateev, V. V. Popov, and M. S. Shur, Semiconductors **44**, 1406–1413 (2010).
 - [23] D. Fateev, K. Mashinsky, O. Polischuk, and V. Popov, Phys. Rev. Appl. **11**, 064002 (2019).
 - [24] T. Otsuji, Y. M. Meziani, T. Nishimura, T. Suemitsu, W. Knap, E. Sano, T. Asano, and V. V. Popov, Journal of Physics: Condensed Matter **20**, 384206 (2008).
 - [25] T. Otsuji, T. Watanabe, S. A. Boubanga Tombet, A. Satou, W. M. Knap, V. V. Popov, M. Ryzhii, and V. Ryzhii, IEEE Trans. Terahertz Sci. Technol. **3**, 63 (2013).
 - [26] P. Sai, V. V. Korotyeyev, M. Dub, M. Slowikowski, M. Filipiak, D. B. But, Y. Ivonyak, M. Sakowicz, Y. M. Lyaschuk, S. M. Kukhtaruk, G. Cywiński, and W. Knap, Phys. Rev. X **13**, 041003 (2023).
 - [27] I. V. Gorbenko and V. Y. Kachorovskii, “Lateral plasmonic crystals: Tunability, dark modes, and weak-to-

- strong coupling transition,” (2024).
- [28] W. Knap, V. Kachorovskii, Y. Deng, S. Rumyantsev, J.-Q. Lü, R. Gaska, M. S. Shur, G. Simin, X. Hu, M. A. Khan, C. A. Saylor, and L. C. Brunel, *Journal of Applied Physics* **91**, 9346–9353 (2002).
- [29] A. Zak, M. A. Andersson, M. Bauer, J. Matukas, A. Lisauskas, H. G. Roskos, and J. Stake, *Nano Letters* **14**, 5834–5838 (2014).
- [30] L. Vicarelli, M. S. Vitiello, D. Coquillat, A. Lombardo, A. C. Ferrari, W. Knap, M. Polini, V. Pellegrini, and A. Tredicucci, *Nature Materials* **11**, 865–871 (2012).
- [31] D. A. Bandurin, I. Gayduchenko, Y. Cao, M. Moskotin, A. Principi, I. V. Grigorieva, G. Goltsman, G. Fedorov, and D. Svintsov, *Applied Physics Letters* **112** (2018), 10.1063/1.5018151.
- [32] J. A. Delgado-Notario, V. Clericò, E. Diez, J. E. Velázquez-Pérez, T. Taniguchi, K. Watanabe, T. Otsuji, and Y. M. Meziani, *APL Photonics* **5**, 066102 (2020).
- [33] J. A. Delgado-Notario, W. Knap, V. Clericò, J. Salvador-Sánchez, J. Calvo-Gallego, T. Taniguchi, K. Watanabe, T. Otsuji, V. V. Popov, D. V. Fateev, E. Diez, J. E. Velázquez-Pérez, and Y. M. Meziani, *Nanophotonics* **11**, 519–529 (2022).
- [34] A. Soltani, F. Kuschewski, M. Bonmann, A. Generalov, A. Vorobiev, F. Ludwig, M. M. Wiecha, D. Čibiraitė, F. Walla, S. Winnerl, S. C. Kehr, L. M. Eng, J. Stake, and H. G. Roskos, *Light: Science, Applications* **9** (2020).
- [35] D. Veksler, F. Teppe, A. P. Dmitriev, V. Y. Kachorovskii, W. Knap, and M. S. Shur, *Phys. Rev. B* **73**, 125328 (2006).
- [36] C. Drexler, N. Dyakonova, P. Olbrich, J. Karch, M. Schaffberger, K. Karpierz, Y. Mityagin, M. B. Lifshits, F. Teppe, O. Klimenko, and et al., *Journal of Applied Physics* **111**, 124504 (2012).
- [37] K. S. Romanov and M. I. Dyakonov, *Applied Physics Letters* **102**, 153502 (2013).
- [38] I. V. Gorbenko, V. Y. Kachorovskii, and M. S. Shur, *physica status solidi (RRL) – Rapid Research Letters* **13**, 1800464 (2019).
- [39] I. V. Gorbenko, V. Y. Kachorovskii, and M. Shur, *Optics Express* **27**, 4004 (2019).
- [40] E. L. Ivchenko and S. D. Ganichev, *JETP Letters* **93**, 673–682 (2011).
- [41] I. V. Rozhansky, V. Y. Kachorovskii, and M. S. Shur, *Phys. Rev. Lett.* **114**, 246601 (2015).
- [42] P. Faltermeier, G. V. Budkin, J. Unverzagt, S. Hubmann, A. Pfaller, V. V. Bel'kov, L. E. Golub, E. L. Ivchenko, Z. Adamus, G. Karczewski, T. Wojtowicz, V. V. Popov, D. V. Fateev, D. A. Kozlov, D. Weiss, and S. D. Ganichev, *Phys. Rev. B* **95**, 155442 (2017).
- [43] P. Faltermeier, G. Budkin, S. Hubmann, V. Bel'kov, L. Golub, E. Ivchenko, Z. Adamus, G. Karczewski, T. Wojtowicz, D. Kozlov, D. Weiss, and S. Ganichev, *Physica E: Low-dimensional Systems and Nanostructures* **101**, 178 (2018).
- [44] S. Hubmann, V. V. Bel'kov, L. E. Golub, V. Y. Kachorovskii, M. Drienovsky, J. Eroms, D. Weiss, and S. D. Ganichev, *Physical Review Research* **2**, 033186 (2020).
- [45] P. Sai, S. O. Potashin, M. Szola, D. Yavorskiy, G. Cywiński, P. Prystawko, J. Łusakowski, S. D. Ganichev, S. Rumyantsev, W. Knap, and V. Y. Kachorovskii, *Physical Review B* **104**, 045301 (2021).
- [46] E. Mönch, S. O. Potashin, K. Lindner, I. Yahniuk, L. E. Golub, V. Y. Kachorovskii, V. V. Bel'kov, R. Huber, K. Watanabe, T. Taniguchi, J. Eroms, D. Weiss, and S. D. Ganichev, *Physical Review B* **105**, 045404 (2022).
- [47] E. Mönch, S. O. Potashin, K. Lindner, I. Yahniuk, L. E. Golub, V. Y. Kachorovskii, V. V. Bel'kov, R. Huber, K. Watanabe, T. Taniguchi, J. Eroms, D. Weiss, and S. D. Ganichev, *Physical Review B* **107**, 115408 (2023).
- [48] S. A. Mikhailov, *Phys. Rev. B* **58**, 1517 (1998).